



HAL
open science

Advanced simulation of ultrasonic inspection of welds using Dynamic Ray Tracing

Audrey Gardahaut, Karim Jezzine, Didier Cassereau, Nicolas Leymarie,
Ekaterina Iakovleva

► **To cite this version:**

Audrey Gardahaut, Karim Jezzine, Didier Cassereau, Nicolas Leymarie, Ekaterina Iakovleva. Advanced simulation of ultrasonic inspection of welds using Dynamic Ray Tracing. e-Journal of Nondestructive Testing, 19 (4), 2013. hal-04509996

HAL Id: hal-04509996

<https://hal.science/hal-04509996>

Submitted on 18 Mar 2024

HAL is a multi-disciplinary open access archive for the deposit and dissemination of scientific research documents, whether they are published or not. The documents may come from teaching and research institutions in France or abroad, or from public or private research centers.

L'archive ouverte pluridisciplinaire **HAL**, est destinée au dépôt et à la diffusion de documents scientifiques de niveau recherche, publiés ou non, émanant des établissements d'enseignement et de recherche français ou étrangers, des laboratoires publics ou privés.

Advanced simulation of ultrasonic inspection of welds using Dynamic Ray Tracing

Audrey GARDAHAUT¹, Karim JEZZINE¹, Didier CASSEREAU², Nicolas LEYMARIE¹, Ekaterina IAKOVLEVA¹

¹ CEA, LIST, F-91191 Gif-Sur-Yvette, France

Phone: +33 16908 4026, Fax: +33 16908 7597; E-mail: audrey.gardahaut@cea.fr, karim.jezzine@cea.fr, nicolas.leymarie@cea.fr, ekaterina.iakovleva@cea.fr

² CNRS, UMR 7623, LIP, 15 Rue de l'école de médecine, F-75006, Paris, France; E-mail: didier.cassereau@upmc.fr

Abstract

The interpretation of on-sites inspections of austenitic or bimetallic welds is particularly difficult due to their internal structures. Indeed, skewing and splitting of the ultrasonic beam caused by inhomogeneity and anisotropy of the material may occur. This paper describes a ray-based model for simulating the ultrasonic wave propagation in such structures. The formalism based on dynamic ray tracing system in Cartesian coordinates along a known ray consists in solving eikonal and transport equations. The ray trajectories are obtained through the resolution of a system of linear ordinary differential equations of the first order, whereas the computation of ray amplitude requires solving the so-called paraxial ray tracing system. This method can be applied using a smooth cartography of the weld material properties obtained thanks to image processing techniques. In this case, the orientation of grains at each point of the weld is extracted by interpolation from the cartography. We present here simulation results using this method and comparison to finite element and experimental results.

Keywords: Dynamic Ray Tracing Method, Weld Inspection, Anisotropic and Inhomogeneous media.

1. Introduction

In the nuclear industry, ultrasonic Non Destructive Testing (NDT) techniques are used to control welded joints of the primary circuit of Pressurized Water Reactor (PWR). Those techniques allow the detection, the localisation and the characterization of defects located inside or in the vicinity of bimetallic welds. Because of their polycrystalline structure, some disturbances of the beam such as splitting and skewing [1, 2] can be observed during on-site inspections. Various simulation tools are developed to help understanding the inspection results such as finite element models [3, 4] or ray tracing models [5]. In the CIVA software, a semi-analytic propagation model based on ray theory [6] may be applied on a piecewise description of a weld. The weld being described as a set of several homogeneous domains with a given crystallographic orientation, the ray propagate along a constant direction of energy for a given slowness vector, and the transmitted and refracted coefficients are evaluated at each interface. In this paper, we present a generalisation of this model that takes into account a continuously varying description of the grain orientation in the weld.

2. Context: Ultrasonic simulation of wave propagation in welds

A bimetallic weld located in the primary circuit of nuclear power plants is composed of a ferritic steel and a stainless steel. Its internal organization depends on many parameters such as the shade of steel, the diameter of the electrode, the velocity and the process of the welding. Because of its heterogeneous and anisotropic nature, the inspections are difficult to understand. Figure 1 shows the beam splitting and skewing due to the complexity of the weld structure. These representations of the wave fields and wave fronts have been obtained from through transmission experiments. The emitter was a L60° wedge probe, with a 12.7 mm

diameter at 2 MHz fixed on the weld. The 2D scanning in reception was performed using a 6.7 mm diameter probe associated to a plexiglass cone to improve the spatial resolution.

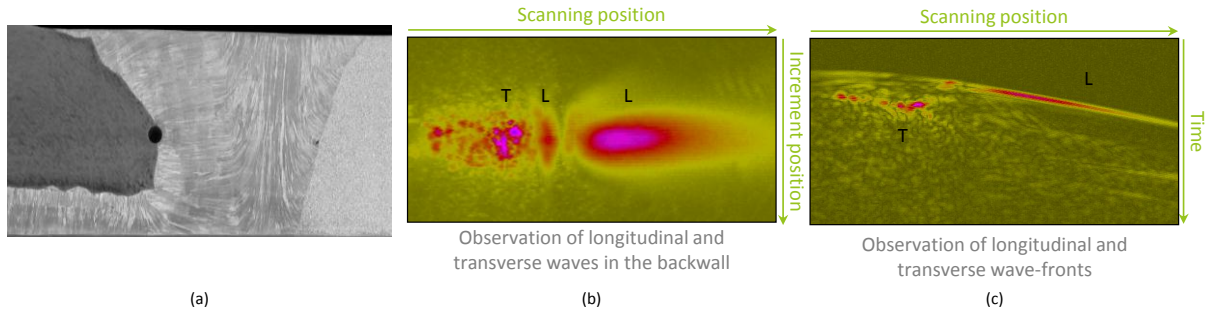


Figure 1: Experimental set-up and results: (a) Macrograph of the weld, (b) Longitudinal and transverse wave amplitudes on the back wall, (c) Longitudinal and transverse wave front at an increment position.

The Dynamic Ray Tracing model (DRT) usually applied in Geophysics [7] has been implemented in order to predict the propagation of ultrasonic waves in such a structure. To perform the simulation, the geometry of the weld, the elasticity constants and the attenuation of the materials and the orientation of the grain at any position in the weld are required. As the DRT relies on a high frequency approximation, it has to be applied on a continuously varying description of the grain orientation in the weld. This may be obtained either in a closed-form [5] or thanks to an image processing technique presented in a previous work [8] as shown in figure 2.

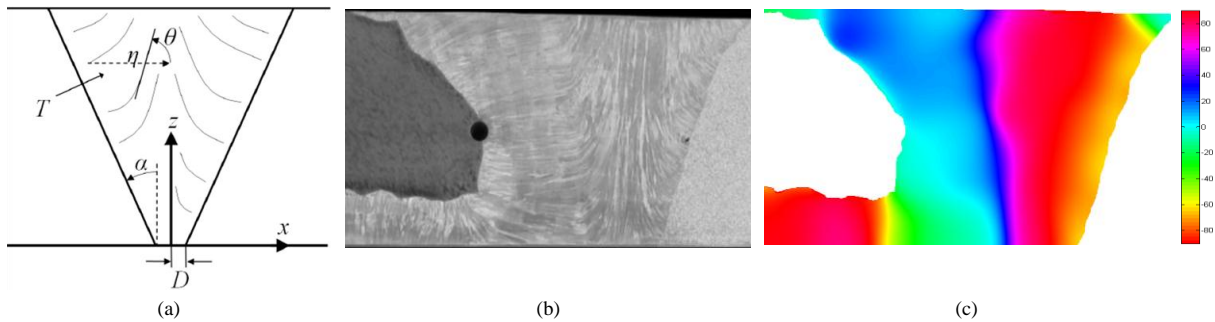


Figure 2: Smooth description of the crystallographic orientation of a weld: (a) Closed-form expression proposed by Ogilvy [5] for a V-shaped weld, (b) Macrograph of a bimetallic weld, (c) Continuously varying description obtained by applying an image processing technique [8] on the macrograph.

The paraxial ray theory is based on the solving of two equations: the *eikonal equation* (1) and the *transport equation* (2). The first one computes the ray-paths and travel-time when the second one evaluates the amplitude of the ray during the propagation. The eikonal equation represents a non-linear partial differential equation of the first order for the travel-time $T(x)$:

$$(\nabla T)^2 = \frac{1}{c(x)^2}. \quad (1)$$

It describes the propagation of the wave front $T(x)$ of the considered wave and depends on the phase velocity $c(x)$ of this wave.

The transport equation represents a linear partial differential equation of the first order in scalar $A(x)$ the amplitude function:

$$A(x)\nabla^2 T(x) + 2\nabla A(x) \cdot \nabla T(x) = 0. \quad (2)$$

It is solved along a ray Ω and describes the conservation of the energy inside the ray tube.

3. Dynamic Ray Tracing Model for smooth description of weld

3.1 Ray theory

The DRT model allows the propagation of ultrasonic waves in anisotropic and inhomogeneous media. By deriving the eikonal equation (1), a differential ray tracing system (3) called the axial ray system is expressed. This system is composed of two coupled ordinary differential equations describing the variations of the position and the slowness with respect to the travel time:

$$\begin{cases} \frac{dx_i}{dT} = a_{ijkl} p_l g_j^{(m)} g_k^{(m)} = V_i^{e(m)}, \\ \frac{dp_i}{dT} = -\frac{1}{2} \frac{\partial a_{ijkl}}{\partial x_i} p_k p_n g_j^{(m)} g_l^{(m)}, \end{cases} \quad (3)$$

where a_{ijkl} are the elasticity constants of the medium at position x_i normalized by the density ρ . p_i represents the components of the slowness vector, $g_j^{(m)}$ are the eigenvectors of the Christoffel tensor corresponding to the polarization vector and $V_i^{e(m)}$ is the energy velocity for a mode m . The solution of system (3) gives the ray trajectories in the weld.

The amplitude of the propagating rays is evaluated by solving the transport equation (2) in inhomogeneous and anisotropic media. By deriving the axial ray system with respect to initial parameter γ , a system of linear ordinary differential equations of the first order for the paraxial quantities $Q_i^{(x)}$ and $P_i^{(x)}$ is obtained (4):

$$\begin{cases} \frac{d}{dT} \left(\frac{dx_i}{d\gamma} \right) = \frac{dQ_i}{dT} = \frac{1}{2} \frac{\partial^2 G}{\partial p_i^{(x)} \partial \gamma} = A_{ij} Q_j + B_{ij} P_j, \\ \frac{d}{dT} \left(\frac{dp_i^{(x)}}{d\gamma} \right) = \frac{dP_i}{dT} = \frac{1}{2} \frac{\partial^2 G}{\partial x_i \partial \gamma} = -C_{ij} Q_j - D_{ij} P_j. \end{cases} \quad (4)$$

The parameter γ represent any parameter of the ray Ω . It can be chosen for example as the take-off angle between the axial and the paraxial rays.

This system called paraxial ray system is expressed with parameter G_m representing the normalized eigenvalues of the Christoffel tensor written as $G_m = a_{ijkl} p_j p_l g_i^{(m)} g_k^{(m)}$. Three eigenvalues are evaluated, associated to three eigenvectors $g_i^{(m)}$ for the three propagating plane waves in the medium.

The axial and paraxial ray systems are solved simultaneously by using numerical techniques (cf. Figure 4) such as the Euler method applied in this case.

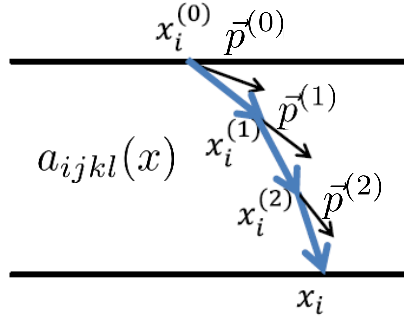


Figure 4: Iterative solving of a ray system.

The expression (4) represents the paraxial ray tracing system in a Cartesian regular coordinates system x_i where the indexes i and j are equal to 1, 2 or 3. In this system, the paraxial ray tracing system consists in six linear ordinary differential equations. It can be written in a wave front orthonormal coordinates system y_i where the indexes M and N take values 1 or 2 [7], such as:

$$\begin{pmatrix} Q_M^{(r+1)} \\ P_M^{(r+1)} \end{pmatrix} = \begin{pmatrix} \Pi_{11} & \Pi_{12} \\ \Pi_{21} & \Pi_{22} \end{pmatrix} \begin{pmatrix} Q_N^{(r)} \\ P_N^{(r)} \end{pmatrix} = \begin{pmatrix} 1 + A_{MN}\Delta T & B_{MN}\Delta T \\ -C_{MN}\Delta T & 1 - D_{MN}\Delta T \end{pmatrix} \begin{pmatrix} Q_N^{(r)} \\ P_N^{(r)} \end{pmatrix} \quad (5)$$

In the wave front coordinates system, the origin moves along the central ray with the propagating wave front. The y_3 -axis is oriented along slowness vector \mathbf{p} at the origin point, and axes y_1 and y_2 are in the plane tangent to the wave front at the origin point and are mutually perpendicular. Expressing the paraxial quantities in the wave front orthonormal coordinates system, allows decreasing the number of linear ordinary differential equations from six to four, simplifying its resolution.

A paraxial ray is thus mathematically written as a vector composed of four paraxial quantities Q_1, Q_2, P_1 and P_2 [7]. Q_1 and Q_2 are the spatial deviation of the paraxial ray from the axial ray and P_1 and P_2 represent the slowness deviation of the paraxial ray from the axial one as shown in figure 5.

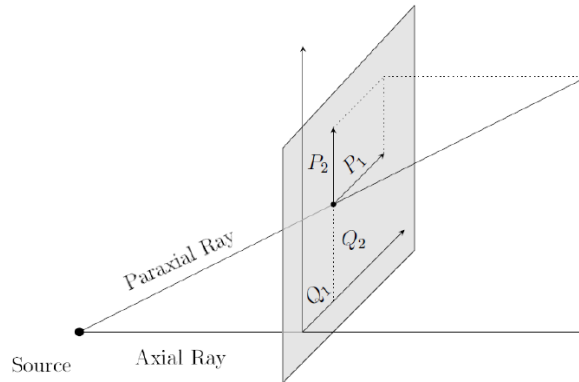


Figure 5: Representation of the paraxial quantities describing a paraxial ray of a tube.

As expressed in expression (5), the paraxial quantities Q_i and P_i at iteration $(r+1)$ are written in function of the same quantities evaluated at the previous iteration (r) through a 4x4 propagation matrix. Then, the paraxial quantities at the last iteration are expressed in function of those at the first iteration through a propagation matrix showing the complete propagation:

$$\begin{pmatrix} Q_M^{(r+1)} \\ P_M^{(r+1)} \end{pmatrix} = L_{(r)} \cdot L_{(r-1)} \cdots L_{(1)} \cdot L_{(0)} \cdot \begin{pmatrix} Q_N^{(0)} \\ P_N^{(0)} \end{pmatrix} = \begin{pmatrix} \Pi_{11_{tot}} & \Pi_{12_{tot}} \\ \Pi_{21_{tot}} & \Pi_{22_{tot}} \end{pmatrix} \begin{pmatrix} Q_N^{(0)} \\ P_N^{(0)} \end{pmatrix} \quad (6)$$

As represented in figure 6, the evolution of the ray tube is followed. The matrices A_{MN} , B_{MN} , C_{MN} and D_{MN} of the propagation matrix are re-evaluated at each time step. Then this propagation matrix is updated and the position and slowness vectors are computed from the axial ray system.

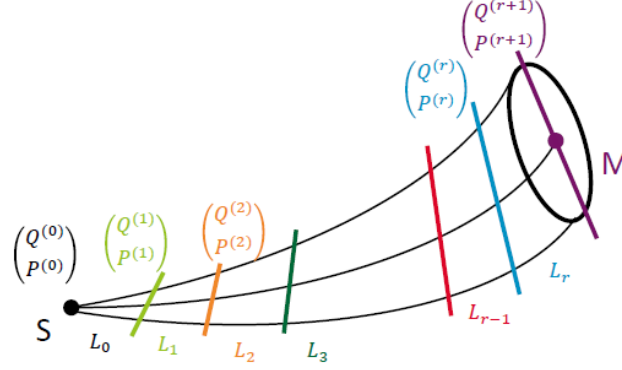


Figure 7: Representation of the evolution of a ray tube and its paraxial quantities Q_i and P_i during the propagation.

Finally, the geometrical spreading \mathcal{L} expressing the evolution of a tube of rays between a source point and a receiver point is evaluated in 3D using the following expression.

$$\mathcal{L}(r+1, 0) = |\det \Pi_{12_{tot}}(r+1, 0)|^{1/2} \quad (7)$$

3.2 Application to a simplified description of the weld

The validation of the model has been made for V-weld with grain orientation described by a closed-form expression (9) proposed by Ogilvy [5]:

$$\theta = \begin{cases} \arctan\left(\frac{T(D+z \tan \alpha)}{x^\eta}\right), & \text{for } x \geq 0, \\ -\arctan\left(\frac{T(D+z \tan \alpha)}{(-x)^\eta}\right), & \text{for } x < 0. \end{cases} \quad (9)$$

Parameters T and α are linked to the geometry of the weld and D and η express the evolution of the orientation of the grain in the weld. As shown in figure 8, the ray trajectories have been validated against the results of Connolly's PhD thesis [10]. In this example, the parameters of the V-weld are: $D = 2\text{mm}$, $\alpha = 21.80^\circ$, $T = 1$ and $\eta = 1$.

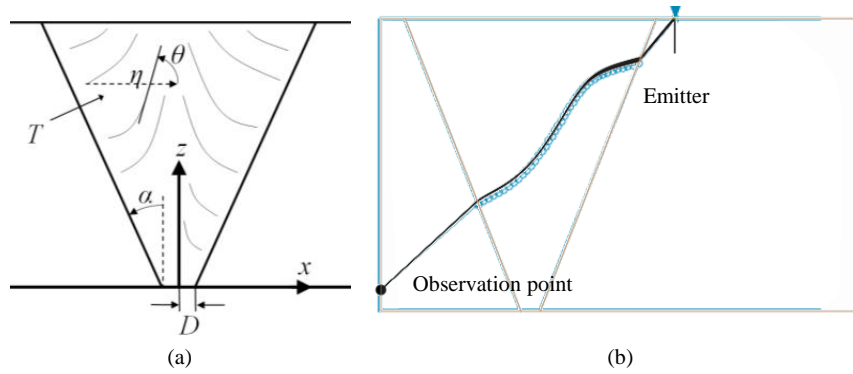


Figure 8: (a) Description of the parameters of the analytical law proposed by Ogilvy [5], (b) Superposition of the ray trajectories obtained by Connolly (oo) and with the dynamic ray tracing model (--).

The ray trajectories evaluated thanks to the axial ray system have been validated with the literature. In order to evaluate the computation of the ray amplitudes via the paraxial ray system, we intend to evaluate the computation made for the wave field for this simplified description of a V-shaped weld. The results obtained with a hybrid finite element code [9] and the DRT are shown in figure 9.

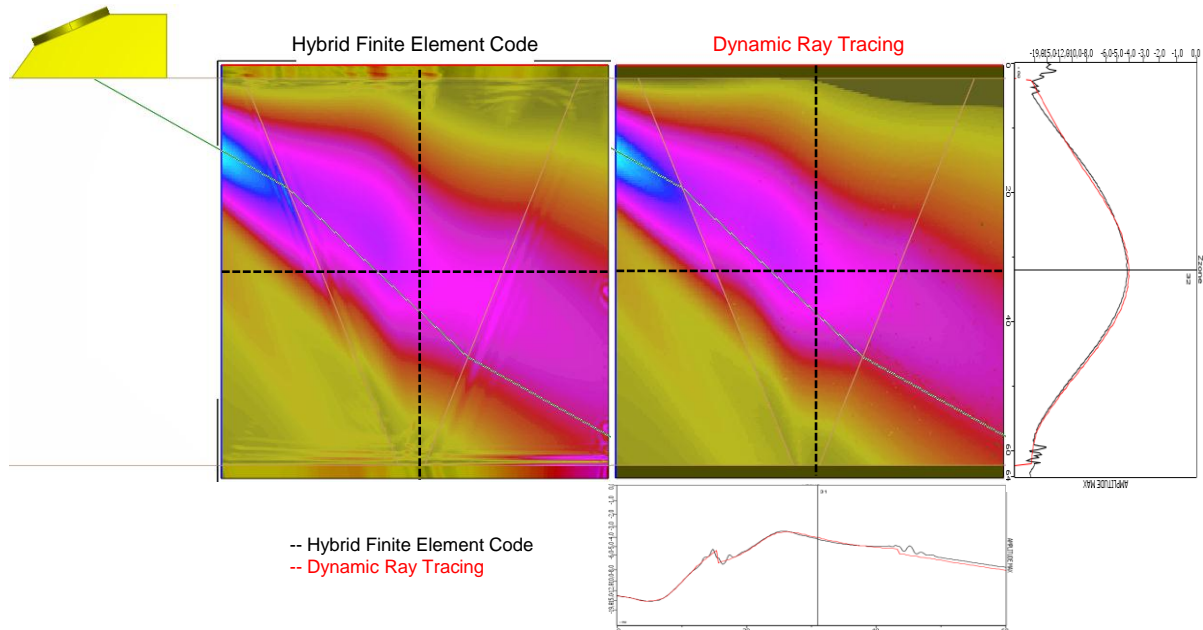


Figure 9: Maximum particle velocity for a weld described by a closed-form expression (Figure 8). Comparison of the results obtained with a 2D hybrid finite element code and a dynamic ray tracing model in 2D.

A good agreement of the computed wave field is observed between the two models for a simplified description of a V-weld. The two systems have been validated for this kind of smooth description of the weld. The next step is to evaluate the model for a realistic description of a weld.

3.3 Application to a realistic description of the weld

In a previous work [8], an image processing technique applied on a macrograph has been exposed in order to obtain a continuously varying description of the grain orientation in a weld. The description is then used as an input data of the numerical models. We have compared this computed wave field for the weld presented in figure 2. Results are shown in figure 10.

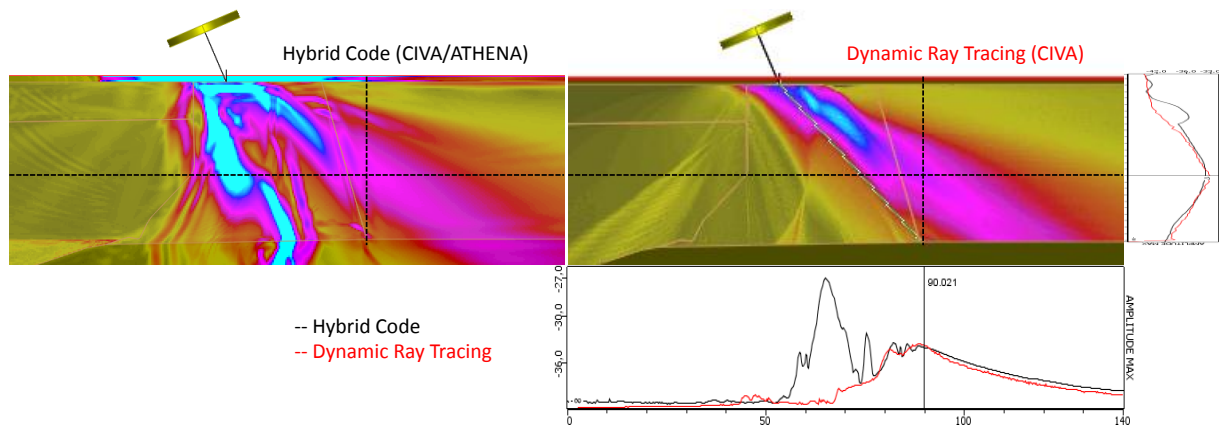


Figure 10: Maximum particle velocity in 2D for a weld described by a cartography of the orientation (Figure 2). Comparison of the results from a hybrid finite element code and a dynamic ray tracing model.

In the simulation, we have only evaluated the propagation of the longitudinal wave in the weld. As for a simplified description of the weld, a good agreement between both computed wave fields obtained with the hybrid finite element code and the dynamic ray tracing model is observed.

4. Conclusions and perspectives

A paraxial ray tracing model has been developed in order to evaluate the ultrasonic propagation in anisotropic and inhomogeneous media. This model is applied on a continuously varying description of the weld. Firstly, it has been validated for a V-shaped weld described with a closed-form expression. The ray trajectories have been successfully compared to the literature. The longitudinal wave field evaluated from these trajectories has been validated with results obtained with a hybrid finite element code. Secondly, the dynamic ray tracing has been applied on a V-shaped weld described with a continuously varying description of the orientations of the grain. A good agreement has been observed between the longitudinal wave field computed with the ray-based model and the hybrid finite element code.

We are currently working on numerical validations of the transverse wave propagation by comparing results obtained with these two models. Furthermore, comparisons between simulations made with the dynamic ray tracing model and experimental results are in progress in order to validate completely the model in 3D. Then, we intend to improve the computation time and the numerical precision by using higher-order numerical methods such as the common fourth-order Runge-Kutta method.

References

1. B Chassignole, O Dupond, L Doudet, V Duwig and N Etchegaray, 'Ultrasonic examination of austenitic weld: illustration of the disturbances of the ultrasonic beam', QNDE, Vol 28, pp 1886-1893, 2009.
2. F Ahmed, 'Etude de la diffusion des ondes ultrasonores dans les soudures austéno-ferritiques: application à la caractérisation des échos de lignes observés lors du contrôle des soudures bimétalliques', Ph.D. Thesis, Université Paris Diderot - Paris 7, 1999.

3. B Chassignole, D Villard, G Ngyuen Van Chi, N Gengembre and A Lhémery, 'Ultrasonic propagation in austenitic stainless steel welds – Approximate model and numerical results and comparison with experiments', QNDE, Vol 19, pp 153-160, 2000.
4. P Fellingner, R Marklein K J Langenberg and S Klaholz, 'Numerical modeling of elastic wave propagation and scattering with EFIT - elastodynamic finite integration technique', Wave Motion, Vol 21, pp 47-66, 1995.
5. J A Ogilvy, 'Computerized ultrasonic ray tracing in austenitic steel', NDT International, Vol 18, No 2, pp67-77, 1985.
6. N Gengembre and A Lhémery, 'Pencil method in elastodynamics: application to ultrasonic field computation', Ultrasonics, Vol 38, pp495-499, 2000.
7. V Červený, 'Seismic ray Theory', Cambridge University Press, 2001.
8. A Gardahaut, K Jezzine and D Cassereau, 'Modelling tools for ultrasonic inspection of bimetallic welds', Proceedings of the Acoustics 2012 Nantes Conference, 2012.
9. S Mahaut, N Leymarie, C Poidevin, T Fouquet and O Dupond, 'Study of complex ultrasonic NDT cases using hybrid simulation method and experimental validations', Insight, Vol 53, pp 664-667, 2011.
10. G D Connolly, 'Modelling of the propagation of ultrasound through austenitic welds', Ph.D. Thesis Imperial College London, 2009.